Quantum Elliptic Vortex in a Nematic-Spin Bose-Einstein Condensate

Hiromitsu Takeuchi *

Department of Physics and Nambu Yoichiro Institute of Theoretical and Experimental Physics (NITEP), Osaka City University, Osaka 558-8585, Japan

(Received 8 September 2020; accepted 9 April 2021; published 12 May 2021)

We find a novel topological defect in a spin-nematic superfluid theoretically. A quantized vortex spontaneously breaks its axisymmetry, leading to an elliptic vortex in nematic-spin Bose-Einstein condensates with small positive quadratic Zeeman effect. The new vortex is considered the Joukowski transform of a conventional vortex. Its oblateness grows when the Zeeman length exceeds the spin healing length. This structure is sustained by balancing the hydrodynamic potential and the elasticity of a soliton connecting two spin spots, which are observable by *in situ* magnetization imaging. The theoretical analysis clearly defines the difference between half quantum vortices of the polar and antiferromagnetic phases in spin-1 condensates.

DOI: 10.1103/PhysRevLett.126.195302

Topological defects (TDs) caused by spontaneous symmetry breaking (SSB) phase transition is ubiquitous, existing as skyrmions in spintronic devices [1], vortices in superconductors and superfluids [2,3], and even disclinations in LCD displays [4]. Thanks to the universal concept of SSB, TDs in laboratories are useful for simulating TDs in other exotic settings, the early Universe, the dense matters in compact stars, and higher-dimensional spacetimes in field theory [5–8]. Multicomponent superfluids with spin freedom, such as spin-triplet superfluid ^{3}He and binary and spinor Bose-Einstein condensates (BECs) [9–12], are powerful tools to develop theories of TDs since various TDs are realized there. Such superfluids are called the nematic-spin superfluids [13], whose order state is partly represented by a vector $\hat{\boldsymbol{d}}$ that mimics the *director* $\tilde{\boldsymbol{d}}$ in nematic liquid crystals (NLCs) [4].

Nematic-spin superfluids support not only conventional TDs in NLCs (disclination, hedgehog, domain wall, and boojum [14–24]), but also novel TDs combined with the superfluidity, e.g., half quantum vortex (HQV) [25]. The term HQV is used also in exciton-polariton condensates [26,27]. The simplest type of HQV has been realized experimentally in different superfluids [28–30], where the core of a vortex in a spin component is occupied by other components. A nontrivial HQV is terminated by a domain wall across which the order-parameter phase jumps by π. The wall-HQV composites were first realized as the double-core vortices in ^{3}He-B [31] and revisited [32–34], motivated by the early Universe scenario nucleating the composites of the Kibble-Lazarides-Shafi (KLS) walls and cosmic strings [35–37]. Recently, the nonequilibrium dynamics of wall-HQV composites were observed in phase transition from the antiferromagnetic (AF) phase to the polar (P) phase [38] in a spin-1 ^{23}Na BEC [39,40]. However, the dynamics are poorly understood, because of the lack knowledge about properties of wall-HQV composites. Determining these properties is important for understanding KLS-wall-HQV composites and double-core vortices in ^{3}He-B [41–45]), the Berezinskii-Kosterlitz-Thouless transition in spinor BECs [46–48], and even the quark-confinement problem in hadronic physics connected with the vortex-confinement problem [49–52].

Here, it is theoretically shown that a wall-HQV composite in spin-1 BECs [39,40] takes an exotic state in equilibrium with a small positive quadratic Zeeman effect. This state, called the elliptic vortex, is hydrodynamically considered the Joukowski transform of a conventional vortex and has an elliptic structure with spin spots (Fig. 1). The spots are confined to the elliptic-vortex core and stabilized by a balance between the hydrodynamic effect and the tension of a domain wall or a soliton spanned between the spots.

Formulation.—A spin-1 BEC is described by the condensate wave function $\Phi_m (m = 0, \pm 1)$ of the $|m\rangle$ Zeeman component in the Gross-Pitaevskii model [12,53]. The thermodynamic energy is represented as $G(\{\Phi_m\}) = \int d^3x\mathcal{G}$, with $\mathcal{G} = (\hbar^2/2M)\sum_m |\nabla\Phi_m|^2 + \mathcal{U}$, and

$$\mathcal{U} = \frac{c_0}{2}n^2 + \frac{c_2}{2}\boldsymbol{s}^2 - (\mu - q)n - q|\Phi_0|^2 - ps_z. \quad (1)$$

Here, we introduced the chemical potential $\mu(> 0)$ and the coefficient q (p) of the quadratic (linear) Zeeman effect. In the Cartesian representation $\Phi = [\Phi_x, \Phi_y, \Phi_z]^T = [(-1/\sqrt{2})(\Phi_{+1} - \Phi_{-1}), (-i/\sqrt{2})(\Phi_{+1} + \Phi_{-1}), \Phi_0]^T$ [54], the condensate density is expressed by the dot product $n = \sum_m |\Phi_m|^2 = \boldsymbol{\Phi}^* \cdot \boldsymbol{\Phi}$ and the spin density by the cross product $\boldsymbol{s} = [s_x, s_y, s_z]^T = i\Phi \times \boldsymbol{\Phi}^*$.

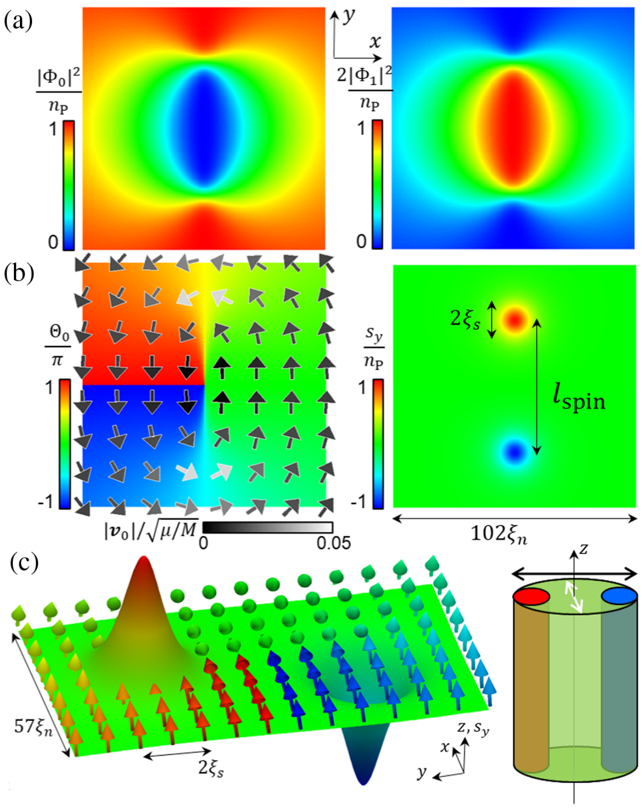

FIG. 1. The cross-sectional profile of an elliptic vortex for $q/\mu = 2^{-17} \approx 7.6 \times 10^{-6}$. (a) The left and right sides show the profiles of $|\Phi_0|^2/n_P$ and $|\Phi_1|^2/(2n_P)$, respectively. The density $|\Phi_{-1}|^2$ (not shown) is the same as $|\Phi_1|^2$. (b) The vector field on the left shows $\boldsymbol{v}_0 = (\hbar/M)\nabla\Theta_0$, with the background plot of $\Theta_0 = \arg\Phi_0$. The phase $\arg\Phi_{\pm 1}$ is homogeneous inside the core (not shown). The spin density s_y is plotted on the right, while $s_x = s_z = 0$. (c) Left: the texture of the unit vector $\boldsymbol{g}/|\boldsymbol{g}|$ (arrow) in Eq. (3). The color of the arrows and the surface correspond to Θ_0 and s_y in (b), respectively. Right: schematic of the three-dimensional structure of the vortex core. The distance $l_{\rm spin}$ between the two spin spots with opposite transverse magnetization (blue and red) is determined by the balance between the hydrodynamic potential and the elastic potential by the AF soliton (green). The width ($\sim l_{\rm spin}$) and thickness of the core are represented by black and white arrows, respectively.

The ground (bulk) state is obtained by minimizing $U = \int d^3x\mathcal{U}$. Assuming $c_2 = 0.016c_0 > 0$ with $p = 0$ obtained experimentally [39,40], the ground state is in the P state $\Phi = \boldsymbol{\Phi}_P = [0, 0, \sqrt{n_P}e^{i\theta_G}]^T$ with the bulk density $n_P = (\mu/c_0)$ and the order-parameter phase θ_G. By rescaling energy and length by μ and $\xi_n \equiv (\hbar/\sqrt{M\mu})$, respectively, the P phase is parametrized by two dimensionless quantities (c_2/c_0) and (q/μ).

Vortex core structure.—One might expect that there is nothing strange about the occurrence of vortices in P phase, whose order parameter (OP) is a complex scalar $\Phi_0 (= \Phi_z)$ with $\Phi_{\pm 1} = 0$, as in conventional superfluids. However, the core of a singly quantized vortex can be unconventional in multicomponent superfluids, occupied by other components so as to reduce the condensation energy, e.g., ^{3}He-B at high pressure [55] and segregated binary BECs [56]. Similarly, the vortex core can be occupied by the $m = \pm 1$ component in the P phase.

To examine the conjecture, the lowest-energy solution was obtained by numerically minimizing G in the steepest descent method [57]. It is found that a nonaxisymmetric core structure is observed for small q/μ. Figure 2 shows the typical cross-sectional profile of the vortex for $(q/\mu) = 2^{-17}$ in a cylindrical flat-bottom potential of sufficiently large radius [58]. The vortex core is occupied by the $m = \pm 1$ components, and the density n is mostly homogeneous [Fig. 1(a)]. Surprisingly, the velocity field forms an elliptic structure, and two spin spots are observed with opposite transverse magnetization ($s_y \neq 0$) at the edges of the core [Fig. 1(b)]. Since the order-parameter phase $\Theta_0 (= \arg\Phi_0)$ jumps by π across the $x = 0$ plane and rotates by π around each spin spot, this structure is regarded as a wall-HQV composite composed of a wall and two HQVs with the same circulation.

The distance $l_{\rm spin}$ between the spin spots is a decreasing function of q [Fig. 2(a)]. Accordingly, the density $n_{\rm core}$ at the center of the vortex core and the maximum spin density $s_\perp^{\rm max}$ decrease with q and vanish at a critical value $q_C \approx 0.25\mu$ [Fig. 2(b)] [59,60]. This behavior is similar to that of the AF-core soliton [61], where the soliton core is vacant for large q but occupied by the local AF state ($\boldsymbol{s} = 0$ with $\Phi_{\pm 1} \neq 0$ and $\Phi_0 \approx 0$) for small q. In our case, however, the vortex core is occupied by two different sates, the local broken-axisymmetry (BA) state ($\boldsymbol{s} \perp \hat{z}$ with $\Phi_1\Phi_0\Phi_{-1} \neq 0$) and the local AF state.

In order to explain the nematic-spin order in the vortex core, we extend the OP space as

$$\boldsymbol{\Phi} = \sqrt{n}e^{i\theta_G}\hat{\boldsymbol{d}}, \tag{2}$$

which represents the OP in the ground state with $\boldsymbol{s} = 0$ for $q = 0$. The real unit vector $\hat{\boldsymbol{d}}$ is called the *pseudo*-director;

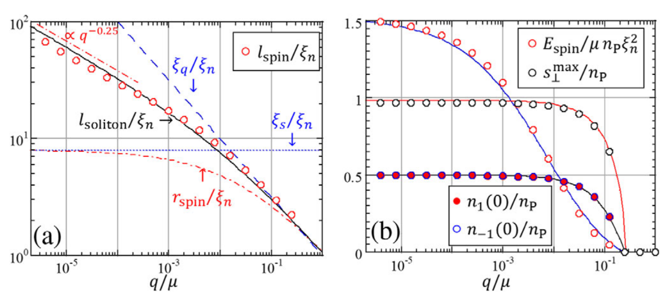

FIG. 2. (a) The q dependence of $l_{\rm spin}$. The solid curve represents the evaluation by Eq. (12). All lengths are rescaled by ξ_n. (b) The q dependence of the spin interaction $E_{\rm spin}$, the maximum spin density $s_\perp^{\rm max} = \max(s_y)$, and the core density $n_{\pm 1}(0)$. The solid curve tracing the data corresponds to an analytic formula (see text).

the state of $(\hat{\boldsymbol{d}}, \theta_G)$ is identical to $(-\hat{\boldsymbol{d}}, \theta_G + \pi)$. In terms of the extended OP, the ground state in the P (AF) phase with $q > 0$ ($q < 0$) is represented as $n = n_P$ and $\hat{\boldsymbol{d}} = \pm\hat{\boldsymbol{z}}$ ($n = n_{\rm AF}$ and $\hat{\boldsymbol{d}} = \hat{\boldsymbol{r}}_\perp$) within the unit vector $\hat{\boldsymbol{z}}$ ($\hat{\boldsymbol{r}}_\perp$) parallel (normal) to the quantization axis and the density $n_{\rm AF} = [(\mu - q)/c_0]$ of the AF state. To describe the magnetization together with the nematic-spin order, it is useful to introduce a representation

$$\boldsymbol{\Phi} = e^{i\Theta_0}(\boldsymbol{g} + i\boldsymbol{h}), \qquad (3)$$

with $\boldsymbol{g} = [g_x, g_y, g_z]^T$ with $g_z \geq 0$ and $\boldsymbol{h} \perp \hat{\boldsymbol{z}}$. Equation (3) reduces Eq. (2) for $\boldsymbol{s} = 2\boldsymbol{g} \times \boldsymbol{h} = 0$ with $\boldsymbol{g} = \sqrt{n}\hat{\boldsymbol{d}}$. The left panel in Fig. 1(c) shows a cross-sectional plot of $\boldsymbol{g}/|\boldsymbol{g}|$ and s_y. In the region between the spin spots, $\boldsymbol{g}$ lies on the xy plane forming the local AF state, where the state $(\hat{\boldsymbol{d}}, \Theta_0) = (-\hat{\boldsymbol{x}}, \pm\pi)$ for $x > 0$ is identical to $(\hat{\boldsymbol{x}}, 0)$ for $x < 0$ along the yz plane. The nematic-spin order is destroyed when $\hat{\boldsymbol{d}}$ is ill-defined in the spin spots occupied by the local BA state [see the right panel in Fig. 1(c)].

To clarify our problem, the main goal is to answer the following two questions: What causes the axisymmetry breaking? What is the physical mechanism to stabilize the elliptic structure?

Vortex winding rule.—As the answer for the first question, it is claimed that the spin interaction breaks the axisymmetry. To justify the claim logically, we introduce a winding rule of an axisymmetric vortex in spin-1 BECs. We consider a straight vortex along the z axis, the cross section of which is axisymmetric as the ansatz $\Phi_m = f_m(r)e^{iL_m\varphi}$, with radius $r = \sqrt{x^2 + y^2}$, and azimuthal angle φ in cylindrical coordinates. The rule states that L_m is parametrized by the winding numbers L and N, associated with the mass and spin current, respectively, and given by

$$L_m = L + mN \qquad (L, N = 0, \pm1, \pm2, \ldots). \qquad (4)$$

The rule is related to the phase factor $\delta\Theta = (L_{+1} + L_{-1} - 2L_0)\varphi$. By substituting the ansatz into the equation of motion, we have, for the equation of Φ_0, $0 = (h_0 - \mu + c_0 n + c_2 f_{+1}^2 + c_2 f_{-1}^2 + 2c_2 f_{+1} f_{-1} e^{i\delta\Theta}) f_0$. The last term comes from the transverse spin density, and the equation of real function f_m is solved when $e^{i\delta\Theta} = \pm1$, resulting in Eq. (4). Therefore, this rule is applicable for $s_x \neq 0$ or $s_y \neq 0$ with $f_{+1} f_{-1} f_0 \neq 0$ [62].

By contraposition of the above argument, the vortex must be nonaxisymmetric, when the winding rule is not satisfied. As seen in Fig. 1, only the $m = 0$ component has a nonzero winding number, corresponding to $L_0 = 1$ and $L_{\pm1} = 0$. Such a set of winding numbers cannot satisfy the winding rule. The axisymmetry is exactly recovered only for $\Phi_{\pm1} = 0$ ($q \geq q_C$). Since the winding rule works for $s_x \neq 0$ or $s_y \neq 0$, the transverse magnetization appear as a manifestation of the axisymmetry breaking. The orientations of the transverse spin and the axes of the elliptic structure depend on the phases $\arg \Phi_m$.

Joukowski mapping.—To answer the second question, the potential flow theory in two-dimensional flow is extended to our problem. The elliptic core structure hints at the Joukowski transformation [63], since the velocity field on the cross section is considered a two-dimensional potential flow. This perception is the motivation for investigating the problem, and the following analysis leads to a quantitative evaluation of the core structure.

The velocity field $\boldsymbol{v}_0 = (\hbar/M)\nabla\Theta_0 = (u, v)$ in the xy plane is generated by a conformal mapping called the Joukowski transformation from a vortex within a cylinder of radius a in the ζ complex plane to the xy plane, $x + iy = \zeta + (a^2/\zeta)$ [63]. By using the parametrization $\zeta = iae^{\phi + i\psi}$ $(\phi \geq 0)$, one obtains $(x, y) = 2a(\cosh\phi\cos(\psi + \pi), \sinh\phi\sin(\psi + \pi))$, representing an ellipse of width $4a\cosh\phi$ and thickness $4a\sinh\phi$.

The velocity field is computed by applying the conformal mapping to the complex velocity potential W of the vortex in the ζ plane,

$$W = -i\frac{\kappa}{2\pi}\log\zeta. \qquad (5)$$

The circulation $\kappa = (2\pi\hbar)/M$ around a quantized vortex is conserved in the transformation as follows. By applying the transformation to Eq. (5) and using the formula $v \to \pm(\kappa/2\pi)(1/\sqrt{4a^2 - y^2})$ for $|y| < 2a$ in the limit $x \to \pm0$, the vorticity $\omega_z(x, y) = (\nabla \times \boldsymbol{v}_0)_z$ forms a segment singularity of width $4a$,

$$\omega_z(\boldsymbol{r}) = \frac{\kappa}{\pi}\frac{1}{\sqrt{4a^2 - y^2}}\delta(x)\Theta(2a - |y|), \qquad (6)$$

with the step function Θ ($\Theta = 1$ for $2a \geq |y|$ and $\Theta = 0$ for $2a < |y|$). By integrating Eq. (6), it is confirmed that the circulation is conserved as $\int dxdy\omega_z = \kappa$.

Hydrodynamic potential.—To reveal the physical mechanism that stabilizes the elliptic vortex, the energy $E_{\rm vortex}$ of a vortex of unit length is evaluated. The vortex energy in the ζ plane is computed conventionally by considering the contribution from the core region ($|\zeta| < \rho_{\rm core} \equiv ae^{\phi_{\rm core}}$) and the outer region ($|\zeta| > \rho_{\rm core}$) separately [3]. Similarly, we consider the Joukowski mapping of the former and the latter, corresponding to an ellipse of area $S_{\rm core}$ and outer area $S_{\rm out}$ in the xy plane, respectively.

The core region is characterized by two parameters a and $r_{\rm core} \equiv \rho_{\rm core} - a$ as

$$S_{\rm core} = \pi R_+ R_- = \pi\frac{(a + r_{\rm core})^4 - a^4}{(a + r_{\rm core})^2}, \qquad (7)$$

with $R_\pm = \{[(a + r_\mathrm{core})^2 \pm a^2]/(a + r_\mathrm{core})\}$. Here, $2R_{+(-)}$ is the width (thickness) of the ellipse. For high oblateness with $(a/r_\mathrm{core}) \gg 1$, we have $R_+ \approx 2a$ and $R_- \approx 2r_\mathrm{core}$. The axisymmetric limit $(a/r_\mathrm{core}) \to 0$ results in $R_+ = R_- \to r_\mathrm{core}$.

The vortex energy is defined as the excess energy in the presence of the vortex, with respect to the bulk energy $E_\mathrm{bulk} = \mathcal{U}_P(S_\mathrm{in} + S_\mathrm{out})$ with energy density $\mathcal{U}_P = -\frac{1}{2}\mu n_P$ in the bulk P phase. The vortex energy is then represented formally by

$$E_\mathrm{vortex} = E_\mathrm{out} + E_\mathrm{core} - E_\mathrm{bulk} = U_\mathrm{core} + U_\mathrm{out}, \quad (8)$$

with $E_\mathrm{core(out)} = \int_{S_\mathrm{core(out)}} dxdy\mathcal{G}$ and $U_\mathrm{core(out)} = E_\mathrm{core(out)} - \mathcal{U}_P S_\mathrm{core(out)}$. The potential U_out of the outer region is evaluated by computing the integral in E_out analytically with an approximation $n \approx n_P[1 - (M/2\mu)\boldsymbol{v}_0^2]$, where the quantum pressure is neglected. In the approximation up to the order of $\mathcal{O}[(M/2\mu)\boldsymbol{v}_0^2]$, a straightforward computation yields

$$U_\mathrm{out} \approx U_\mathrm{hyd} = \frac{M n_P \kappa^2}{4\pi} \ln \frac{R}{a + r_\mathrm{core}}. \quad (9)$$

Here, we used the radius $R = ae^{\phi_\mathrm{out}}$ of the system boundary by assuming $R \gg a$ [58].

Elastic core potential.—The core potential U_core is determined by introducing a phenomenological model, where a soliton is spanned between the spin spots. This model is justified by the fact that the phase gradient is mainly concentrated around the spin spots, consistent with the vorticity distribution (6) [see also Fig. 1(b)]; thus, the core structure between the spots is similar to that of the AF-core soliton [61]. Accordingly, we write

$$U_\mathrm{core} = E_\mathrm{soliton} + E_\mathrm{spin}, \quad (10)$$

where the soliton energy E_soliton is a function of the soliton length $l_\mathrm{soliton} \sim l_\mathrm{spot}$ and the spin interaction E_spin comes from the second term of Eq. (1).

The spin interaction is determined independently from the hydrodynamic argument, and thus U_core depends explicitly on l_spot through E_soliton. The size r_spin and the magnitude $s_\perp^\mathrm{max} = \max(s_y)$ of the spin spot are asymptotic to $\xi_s = (\hbar/\sqrt{Mc_2n_P})$ and n_P, respectively, for $\xi_q \gg \xi_s \gg \xi_n$. For $\xi_s \gg \xi_q \gtrsim \xi_n$, the core density grows as $n_{\pm 1}(0) \propto 1 - (q/q_C)$ in the continuous phase transition [64], and the size r_spin must be bounded below the vortex core size $\lesssim \xi_q$. Therefore, the size of a spin spot is simply parametrized as

$$r_\mathrm{spin}^{-1} = \xi_s^{-1} + C_\mathrm{spin}\xi_q^{-1}, \quad (11)$$

with $C_\mathrm{spin} \sim \mathcal{O}(1)$. In fact, the spin interaction, estimated by $E_\mathrm{spin} = \frac{1}{2}c_2(s_y^\mathrm{max})^2\pi r_\mathrm{spin}^2$, agrees well with the numerical result with $C_\mathrm{spin} = 0.8$ [Fig. 2(b)] [58].

To simplify the analysis, we write as $l_\mathrm{soliton} \equiv 4a + 4r_\mathrm{core}$. The equilibrium length is then determined by $(\partial/\partial l_\mathrm{soliton})E_\mathrm{vortex} = (\partial/\partial l_\mathrm{soliton})(U_\mathrm{hyd} + E_\mathrm{soliton}) = 0$. In the first approximation, the soliton energy E_soliton is expressed as $E_\mathrm{soliton}^\mathrm{first} = \alpha_\mathrm{AF} l_\mathrm{soliton}$ with the tension coefficient $\alpha_\mathrm{AF} \sim \sqrt{q\mu} n_P \xi_n$ of the AF-core soliton [61]. This approximation fails for $\xi_q \gg \xi_s$. Actually, the thickness of the elliptic core is much smaller than the thickness $\sim\xi_q$ of the AF-core soliton forming a halo structure [Fig. 1(a)], which increases the tension effectively. To take this effect into account, we introduce a phenomenological formula

$$\frac{E_\mathrm{soliton}}{\mu n_P \xi_n^2} = \sqrt{\frac{q}{\mu}} \frac{l_\mathrm{soliton}}{\xi_n}\left(1 + \frac{l_\mathrm{soliton}}{r_\mathrm{spin}}\right). \quad (12)$$

This formula yields $(l_\mathrm{soliton}/\xi_n) = (r_\mathrm{spin}/4\xi_n)[\sqrt{1 + 8\pi(\xi_q/r_\mathrm{spin})} - 1]$ and explains the scaling behavior $l_\mathrm{soliton} \sim l_\mathrm{spin} \propto q^{-0.25}$ for $\xi_q \gg \xi_s$ in Fig. 2(a). This means that the soliton is effectively elastic with $E_\mathrm{soliton} \propto l_\mathrm{soliton}^2$ for $l_\mathrm{spin} \gg r_\mathrm{spin}$.

Rotating solutions.—Finally, the response to an external rotation is investigated as a dynamical property. The external rotation of angular frequency Ω is described by the energy in the rotating frame $G' = G - \Omega L_z$, with the angular momentum L_z along the z axis [65]. The width l_spin^Ω of an elliptic vortex decreases with Ω [Fig. 3(a)], since the angular momentum increases more as the vorticity is localized more toward the center. Owing to the boundary effect [66], the single-vortex states are unstable for large $|\Omega|$ or small q/μ, leading to a lattice of elliptic vortices [inset of Fig. 3(a)].

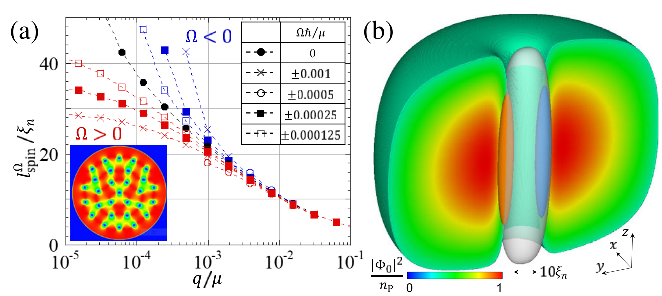

FIG. 3. (a) The q dependence of the width l_spin^Ω of a rotating elliptic vortex with angular velocity Ω. The single vortex is unstable for larger $|\Omega|$ and smaller q due the boundary effect. Inset: an elliptic-vortex lattice obtained after the instability due to the boundary effect for $\Omega\hbar/\mu = 0.001$ and $q/\mu = 2^{-11}$. (b) The three-dimensional solution of an elliptic vortex in a harmonic trap for $\Omega\hbar/\mu = 0.0005$. The isovolume plot shows the region $|\Psi_0|^2 c_0/\mu \le 0.3$ for $x > 0$ with its $x = 0$ cross-sectional profile. A translucent surface along the z axis represents the isosurface of $|\Psi_{\pm 1}|^2 c_0/\mu = 0.15$, to which the two poles of the isosurfaces $s_y c_0/\mu = \pm 0.7$ are attached (red for positive and blue for negative).

The three-dimensional structure of an elliptic vortex is demonstrated numerically for a feasible setup in Fig. 3(b). A ^{23}Na BEC of 5.6×10^5 atoms is in a harmonic trap $V_{\rm trap} = (M/2)(\omega_\perp^2 r^2 + \omega_z^2 z^2)$ with $(\hbar/\mu)(\omega_\perp, \omega_z) \approx (0.019, 0.024)$. The spin spots appear as two poles (red and blue) along the $m = \pm 1$ component (translucent pole) in the vortex core.

Discussion.—Although the wall-HQV composites were thought to be finally unstable, decaying into conventional axisymmetric vortices due to the snake instability of the wall [39,40], the result suggests that they survive as elliptic vortices after the phase transition. The vortices including their dynamics will be observed through the transverse-spin spots by *in situ* magnetization imaging [29]. The theory here can be applied in a similar manner to the double-core vortex or the KLS-wall-HQV composite in ^{3}He-B, while different forms of the hydrodynamic potential and soliton tension were introduced [67].

It is important to make a clear distinction between the types of HQVs in the AF phase (type I) and the P phase (type II). Properties of type-I HQVs are understood by the following correspondence between binary BECs and the AF phase. Since the equation of motion of spin-1 BECs with $\Phi_0 = 0$ reduces to that of binary BECs, HQVs in miscible binary BECs are physically identical to type-I HQVs in the absence of the $m = 0$ component [29]; type-I HQVs with the same circulation are repulsive according to Ref. [68], where the intra- and intercomponent coupling constants correspond to $g_1 = g_2 = c_0 + c_2$ and $g_{12} = c_0 - c_2$, respectively. Therefore, a pair of type-I HQVs are unstable without external rotation [69], which differs from type-II HQVs in that they form a bound pair by the wall tension [70–72].

It should be mentioned that similar composite objects are investigated experimentally as the spin-mass vortex attached by a planar soliton in ^{3}He-B [73,74] and theoretically as the vortex molecules in Rabi-coupled binary BECs [49–52,75–79]. Interestingly, the confinement of vortices by domain walls is considered a toy model of the quark-confinement problem [49]. Accordingly, "HQV-wall plasma" an analog of quark-gluon plasma (QGP), occurs at a finite temperature T at least for $T > (q/k_B)$ in nematic-spin BECs, where thermal fluctuations free the spin spots from the confinement by the AF-core soliton. In this sense, the observed phase-transition dynamics [39,40] are regarded as simulations of the transition dynamics from QGP to hadrons like the big bang simulation in "little bang" [80]. Further investigations on the dynamics and interactions of elliptic vortices will shed light on unexplored phase-transition dynamics in different physical systems.

H. T. thanks Yong-il Shin for discussion and critical reading of the Letter. This work is supported by JSPS KAKENHI Grants No. JP17K05549, No. JP18KK0391, and No. JP20H01842, and in part by the OCU "Think globally, act locally" Research Grant for Young Scientists through the hometown donation fund of Osaka City.

*takeuchi@osaka-cu.ac.jp

[1] R. Wiesendanger, Nanoscale magnetic skyrmions in metallic films and multilayers: A new twist for spintronics, Nat. Rev. Mater. **1**, 16044 (2016).
[2] D. R. Tilley and J. Tilley, *Superfluidity and Superconductivity*, Graduate Student Series in Physics, 2nd ed. (Adam Hilger, 1986).
[3] R. J. Donnelly, *Quantized Vortices in Helium II* (Cambridge University Press, Cambridge, England, 1991), Vol. 2.
[4] S. Chandrasekhar, *Liquid Crystals*, 2nd ed. (Cambridge University Press, Cambridge, England, 1992).
[5] A. Vilenkin and E. P. S. Shellard, *Cosmic Strings and Other Topological Defects* (Cambridge University Press, Cambridge, England, 2000).
[6] D. Page and S. Reddy, Dense matter in compact stars: Theoretical developments and observational constraints, Annu. Rev. Nucl. Part. Sci. **56**, 327 (2006).
[7] T. Vachaspati, *Kinks and Domain Walls: An Introduction to Classical and Quantum Solitons* (Cambridge University Press, Cambridge, England, 2006).
[8] A. Sen, Tachyon dynamics in open string theory, Int. J. Mod. Phys. A **20**, 5513 (2005).
[9] D. Vollhardt and P. Wolfle, *The Superfluid Phases of Helium 3* (Courier Corporation, North Chelmsford, 2013).
[10] G. E. Volovik, *The Universe in a Helium Droplet*, Vol. 117 (Oxford University Press on Demand, New York, 2003).
[11] K. Kasamatsu, M. Tsubota, and M. Ueda, Vortices in multicomponent Bose-Einstein condensates, Int. J. Mod. Phys. B **19**, 1835 (2005).
[12] Y. Kawaguchi and M. Ueda, Spinor Bose-Einstein condensates, Phys. Rep. **520**, 253 (2012).
[13] The term "nematic-spin" or "spin-nematic" has been also used in literature of different condensed matter systems, e.g., the spin-nematic phase in antiferromagnets [H. Tsunetsugu and M. Arikawa, Spin Nematic Phase in $S = 1$ Triangular Antiferromagnets, J. Phys. Soc. Jpn. **75**, 083701 (2006)] andthe nematic-spin fluid in $BaFe_2As_2$ [L. W. Harriger, H. Q. Luo, M. S. Liu, C. Frost, J. P. Hu, M. R. Norman, and P. Dai, Nematic spin fluid in the tetragonal phase of $BaFe_2As_2$, Phys. Rev. B **84**, 054544 (2011)].
[14] N. D. Mermin, The topological theory of defects in ordered media, Rev. Mod. Phys. **51**, 591 (1979).
[15] P. B. Sunil Kumar and G. S. Ranganath, On certain liquid crystal defects in a magnetic field, Mol. Cryst. Liq. Cryst. **177**, 131 (1989).
[16] G. E. Volovik, *Exotic Properties of Superfluid ^{3}He* (World Scientific, Singapore, 1992), Vol. 1.
[17] V. P. Mineyev and G. E. Volovik, Planar and linear solitons in superfluid ^{3}He, Phys. Rev. B **18**, 3197 (1978).
[18] F. Zhou, Spin Correlation and Discrete Symmetry in Spinor Bose-Einstein Condensates, Phys. Rev. Lett. **87**, 080401 (2001).
[19] F. Zhou, Quantum spin nematic states in Bose-Einstein condensates, Int. J. Mod. Phys. B **17**, 2643 (2003).

[20] J. Ruostekoski and J. R. Anglin, Monopole Core Instability and Alice Rings in Spinor Bose-Einstein Condensates, Phys. Rev. Lett. **91**, 190402 (2003).

[21] N. D. Mermin, *Surface Singularities and Superflow in ^{3}He-A* (Springer, Boston, MA, 1977), pp. 3–22.

[22] G. E. Volovik, Defects at interface between *A* and *B* phases of superfluid ^{3}He, JETP Lett. **51**, 449 (1990).

[23] T. Sh. Misirpashaev, The topological classification of defects at a phase interface, Sov. Phys. JETP **72**, 973 (1991).

[24] H. Takeuchi and M. Tsubota, Boojums in rotating two-component Bose-Einstein condensates, J. Phys. Soc. Jpn. **75**, 063601 (2006).

[25] U. Leonhardt and G. E. Volovik, How to create Alice string (half quantum vortex) in a vector Bose-Einstein condensate, Pis'ma Zh. Eksp. Teor. Fiz. **72**, 66 (2000).

[26] Y. G. Rubo, Half Vortices in Exciton Polariton Condensates, Phys. Rev. Lett. **99**, 106401 (2007).

[27] K. G. Lagoudakis, T. Ostatnický, A. V. Kavokin, Y. G. Rubo, R. André, and B. Deveaud-Plédran, Observation of half-quantum vortices in an exciton-polariton condensate, Science **326**, 974 (2009).

[28] M. R. Matthews, B. P. Anderson, P. C. Haljan, D. S. Hall, C. E. Wieman, and E. A. Cornell, Vortices in a Bose-Einstein Condensate, Phys. Rev. Lett. **83**, 2498 (1999).

[29] S. W. Seo, S. Kang, W. J. Kwon, and Y.-il. Shin, Half-Quantum Vortices in an Antiferromagnetic Spinor Bose-Einstein Condensate, Phys. Rev. Lett. **115**, 015301 (2015).

[30] S. Autti, V. V. Dmitriev, J. T. Mäkinen, A. A. Soldatov, G. E. Volovik, A. N. Yudin, V. V. Zavjalov, and V. B. Eltsov, Observation of Half-Quantum Vortices in Topological Superfluid ^{3}He, Phys. Rev. Lett. **117**, 255301 (2016).

[31] Y. Kondo, J. S. Korhonen, M. Krusius, V. V. Dmitriev, Y. M. Mukharsky, E. B. Sonin, and G. E. Volovik, Direct Observation of the Nonaxisymmetric Vortex in Superfluid ^{3}He-B, Phys. Rev. Lett. **67**, 81 (1991).

[32] J. T. Mäkinen, V. V. Dmitriev, J. Nissinen, J. Rysti, G. E. Volovik, A. N. Yudin, K. Zhang, and V. B. Eltsov, Half-quantum vortices and walls bounded by strings in the polar-distorted phases of topological superfluid ^{3}He, Nat. Commun. **10**, 237 (2019).

[33] G. E. Volovik and K. Zhang, String monopoles, string walls, vortex skyrmions, and nexus objects in the polar distorted *B* phase of ^{3}He, Phys. Rev. Research **2**, 023263 (2020).

[34] K. Zhang, One dimensional nexus objects, network of Kibble-Lazarides-Shafi string walls, and their spin dynamic response in polar distorted *B*-phase of ^{3}He, Phys. Rev. Research **2**, 043356 (2020).

[35] T. W. B. Kibble, G. Lazarides, and Q. Shafi, Walls bounded by strings, Phys. Rev. D **26**, 435 (1982).

[36] T. W. B. Kibble, G. Lazarides, and Q. Shafi, Strings in so (10), Phys. Lett. **113B**, 237 (1982).

[37] T. W. B. Kibble, *Topological Defects and the Non-Equilibrium Dynamics of Symmetry Breaking Phase Transitions* (Springer, Netherlands, 2000), Vol. 549.

[38] There are several ways to call phases of spin-1 BECs. In this Letter, we apply the way used in the phase diagram of the review paper [12] (see Fig. 3 and Table 5 therein) with an aim to clearly specify the influence of the Zeeman shift, while the region of antiferromagnetic interaction in the phase diagram is sometimes called "the polar phase" regardless of the Zeeman shift. It is noted that the AF and *P* phases are also called the easy-plane-polar and easy-axis-polar phases, respectively.

[39] S. Kang, S. W. Seo, H. Takeuchi, and Y. Shin, Observation of Wall-Vortex Composite Defects in a Spinor Bose-Einstein Condensate, Phys. Rev. Lett. **122**, 095301 (2019).

[40] S. Kang, D. Hong, J. H. Kim, and Y. Shin, Crossover from weak to strong quench in a spinor Bose-Einstein condensate, Phys. Rev. A **101**, 023613 (2020).

[41] T. Kita, Unconventional vortices and phase transitions in rapidly rotating superfluid ^{3}He, Phys. Rev. B **66**, 224515 (2002).

[42] M. A. Silaev, E. V. Thuneberg, and M. Fogelström, Lifshitz Transition in the Double-Core Vortex in ^{3}He − B, Phys. Rev. Lett. **115**, 235301 (2015).

[43] K. Kasamatsu, R. Mizuno, T. Ohmi, and M. Nakahara, Effects of a magnetic field on vortex states in superfluid $^3\mathrm{He}-B$, Phys. Rev. B **99**, 104513 (2019).

[44] M. Tange and R. Ikeda, Half-quantum vortex pair in the polar-distorted *B* phase of superfluid ^{3}He in aerogels, Phys. Rev. B **101**, 094512 (2020).

[45] R. C. Regan, J. J. Wiman, and J. A. Sauls, Vortex phase diagram of rotating superfluid ^{3}He − B, Phys. Rev. B **101**, 024517 (2020).

[46] S. Mukerjee, C. Xu, and J. E. Moore, Topological Defects and the Superfluid Transition of the $s = 1$ Spinor Condensate in Two Dimensions, Phys. Rev. Lett. **97**, 120406 (2006).

[47] A. J. A. James and A. Lamacraft, Phase Diagram of Two-Dimensional Polar Condensates in a Magnetic Field, Phys. Rev. Lett. **106**, 140402 (2011).

[48] M. Kobayashi, Berezinskii-Kosterlitz-Thouless transition of spin-1 spinor Bose gases in the presence of the quadratic zeeman effect, J. Phys. Soc. Jpn. **88**, 094001 (2019).

[49] D. T. Son and M. A. Stephanov, Domain walls of relative phase in two-component Bose-Einstein condensates, Phys. Rev. A **65**, 063621 (2002).

[50] M. Tylutki, L. P. Pitaevskii, A. Recati, and S. Stringari, Confinement and precession of vortex pairs in coherently coupled Bose-Einstein condensates, Phys. Rev. A **93**, 043623 (2016).

[51] M. Eto and M. Nitta, Confinement of half-quantized vortices in coherently coupled Bose-Einstein condensates: Simulating quark confinement in a QCD-like theory, Phys. Rev. A **97**, 023613 (2018).

[52] A. Gallemí, L. P. Pitaevskii, S. Stringari, and A. Recati, Decay of the relative phase domain wall into confined vortex pairs: The case of a coherently coupled bosonic mixture, Phys. Rev. A **100**, 023607 (2019).

[53] C. J. Pethick and H. Smith, *Bose–Einstein Condensation in Dilute Gases* (Cambridge University Press, Cambridge, England, 2008).

[54] T. Ohmi and K. Machida, Bose-Einstein condensation with internal degrees of freedom in alkali atom gases, J. Phys. Soc. Jpn. **67**, 1822 (1998).

[55] M. M. Salomaa and G. E. Volovik, Vortices with Ferromagnetic Superfluid Core in $^3\mathrm{He}-B$, Phys. Rev. Lett. **51**, 2040 (1983).

[56] S. Hayashi, M. Tsubota, and H. Takeuchi, Instability crossover of helical shear flow in segregated Bose-Einstein condensates, Phys. Rev. A **87**, 063628 (2013).

[57] H. B. Curry, The method of steepest descent for non-linear minimization problems, Q. Appl. Math. **2**, 258 (1944).

[58] See Supplemental Material at http://link.aps.org/supplemental/10.1103/PhysRevLett.126.195302 for details of the numerical method, cross-sectional profiles for different values of q/μ, derivation of the hydrodynamic potential, and computation of the spin interaction.

[59] Neglecting the spin interaction with $(c_1/c_0) = 0.016 \ll 1$, the critical value is determined as $q_C/\mu \approx 0.25$ by regarding $\Phi_{\pm 1}$ as a single-particle wave function bounded by the vortex core of Φ_0. A similar problem is solved for the nematic-spin vortex in the AF phase [60].

[60] A. P. C. Underwood, D. Baillie, P. Blair Blakie, and H. Takeuchi, Properties of a nematic spin vortex in an antiferromagnetic spin-1 Bose-Einstein condensate, Phys. Rev. A **102**, 023326 (2020).

[61] I. Liu, S.-C. Gou, H. Takeuchi, Phase diagram of solitons in the polar phase of a spin-1 Bose-Einstein condensate, Phys. Rev. Research **2**, 033506 (2020).

[62] A similar rule has been introduced in the absence of the quadratic Zeeman effect; T. Isoshima, K. Machida, and T. Ohmi, Quantum vortex in a spinor Bose-Einstein condensate, J. Phys. Soc. Jpn. **70**, 1604 (2001).

[63] L. M. Milne-Thomson, *Theoretical Aerodynamics* (Dover Publications, New York, 2012).

[64] A similar behavior was also found in the continuous phase transition of the core state of soliton and vortex in spinor BECs [60,61].

[65] E. M. Lifshitz and L. P. Pitaevskii, *Statistical Physics, Part 2*, edited by L. D. Landau and E. M. Lifshitz (Pergamon Press, New York, 1980), Vol. 9.

[66] In a rotating frame, the local superfluid velocity at the surface of the condensate is estimated as $\boldsymbol{v}_0 = (v_\varphi - R\Omega)\hat{\boldsymbol{\varphi}}$ with $v_\varphi \sim [\hbar/(MR_\perp)]$. When the velocity exceeds a critical value, comparable to the phonon velocity $\sqrt{\mu/M}$, the vortex nucleation occur after the excitation of ripplons due to the Landau instability at the surface.

[67] G. Volovik, Half-quantum vortices in superfluid ^{3}He-B, JETP Lett. **52**, 358 (1990).

[68] M. Eto, K. Kasamatsu, M. Nitta, H. Takeuchi, and M. Tsubota, Interaction of half-quantized vortices in two-component Bose-Einstein condensates, Phys. Rev. A **83**, 063603 (2011).

[69] J. Lovegrove, M. O. Borgh, and J. Ruostekoski, Energetically stable singular vortex cores in an atomic spin-1 Bose-Einstein condensate, Phys. Rev. A **86**, 013613 (2012).

[70] Although type-II HQVs have been numerically realized under rotation [71,72], they did not distinguish physically type-I and type-II by neglecting the impact of the domain wall.

[71] M. O. Borgh, M. Nitta, and J. Ruostekoski, Stable Core Symmetries and Confined Textures for a Vortex Line in a Spinor Bose-Einstein Condensate, Phys. Rev. Lett. **116**, 085301 (2016).

[72] J. Lovegrove, M. O. Borgh, and J. Ruostekoski, Stability and internal structure of vortices in spin-1 Bose-Einstein condensates with conserved magnetization, Phys. Rev. A **93**, 033633 (2016).

[73] Y. Kondo, J. S. Korhonen, M. Krusius, V. V. Dmitriev, E. V. Thuneberg, and G. E. Volovik, Combined Spin-Mass Vortex with Soliton Tail in Superfluid ^{3}He-B, Phys. Rev. Lett. **68**, 3331 (1992).

[74] O. V. Lounasmaa and E. Thuneberg, Vortices in rotating superfluid 3He, Proc. Natl. Acad. Sci. U.S.A. **96**, 7760 (1999).

[75] K. Kasamatsu, M. Tsubota, and M. Ueda, Vortex Molecules in Coherently Coupled Two-Component Bose-Einstein Condensates, Phys. Rev. Lett. **93**, 250406 (2004).

[76] M. Cipriani and M. Nitta, Crossover between Integer and Fractional Vortex Lattices in Coherently Coupled Two-Component Bose-Einstein Condensates, Phys. Rev. Lett. **111**, 170401 (2013).

[77] L. Calderaro, A. L. Fetter, P. Massignan, and P. Wittek, Vortex dynamics in coherently coupled Bose-Einstein condensates, Phys. Rev. A **95**, 023605 (2017).

[78] K. Ihara and K. Kasamatsu, Transverse instability and disintegration of a domain wall of a relative phase in coherently coupled two-component Bose-Einstein condensates, Phys. Rev. A **100**, 013630 (2019).

[79] M. Kobayashi, M. Eto, and M. Nitta, Berezinskii-Kosterlitz-Thouless Transition of Two-Component Bose Mixtures with Intercomponent Josephson Coupling, Phys. Rev. Lett. **123**, 075303 (2019).

[80] K. Yagi, T. Hatsuda, and Y. Miake, *Quark-Gluon Plasma: From Big Bang to Little Bang* (Cambridge University Press, Cambridge, England, 2005), Vol. 23.